Proceedings of the ASME 2010 3rd Joint US-European Fluids Engineering Summer Meeting and 8th International Conference on Nanochannels, Microchannels, and Minichannels
FEDSM-ICNMM2010
August 1-5, 2010, Montreal, Canada

FEDSM-ICNMM2010-30228

UNSTEADY NUMERICAL RESEARCH INTO THE IMPACT OF BLEEDING ON AXIAL COMPRESSOR PERFORMANCE

Zhao Bin, Li Shaobin, Li Qiushi, Zhou Sheng
National Key Laboratory on Aero-Engines, School of Jet Propulsion
Beijing University of Aeronautics and Astronautics, Beijing 100191, China

ABSTRACT

The cooling gas of turbine components in aero-engine is extracted from the compressor. Its flow rate is related to the temperature before turbine. The percentage is usually about 3-5% and sometimes up to 25% of the main flow. Very few of the current studies in this field touched on the influence of air bleeding on compressor performance. This paper takes the single stage and low speed axial compressor as the research object, develops a time-accurate numerical method on the compressor overall performance by using the moving mesh to simulate the function of compressor throttle plug. Combined with experimental results, compressor flow field with and without air bleeding are compared and analyzed to study the impact of bleeding on compressor performance. The results show that if a bleeding design can ease the blockage generated by the tip leakage flow and the backflow near the trailing edge, the stall will be effectively postponed and the compressor stability margin will be expanded.

INTRODUCTION

Air system is essential to the safe and reliable operation of aircraft engines. Air with proper pressure and temperature is used for cabin air conditioning, engine inlet anti-ice and cooling of high temperature components (1, 2). The research showed that most of the required airflow of the air system came from the compressor exit, and a small part was extracted from the inter-stage of the high-pressure compressor. The former accounts for a large percentage, but the impact on the compressor performance is small enough to be ignored. The bleed air from the high pressure compressor has taken up 3-5% of the main flow (3). Although the percentage is relatively small, the air comes from such an important part of the engine that it will generate great impact on the compressor performance.

During recent years, researchers in the field of turbomachinery have been paying attention to the impact of air bleeding on the compressor performance. Wellborn (4) evaluated the influence of the bleed location on the compressor performance. Lishman and Cumpsty (5, 6 and 7) did a series of studies on the mechanisms of air bleeding in blade passage. They suggested that the interaction of bleed off-takes with the primary passage flow is basically an inviscid and pressure-driven phenomenon. It largely depends on the rate and bleeding off-take location. By analyzing the loss and the performance of compressor after the end wall boundary layer removal, Gummer (8, 9) found that the bleeding can effectively reduce the reverse-flow along the casing and blockage and loss in local region. All these previous studies have shown that it is very likely to improve compressor performance by studying air system bleeding.

The compressor performance can gain a maximum improvement if air bleeding is used to control the flow field behaviors which have negative impact on the compressor. The design point of compressor is usually selected far away from the stall boundary to ensure a sufficient stability margin. If the bleeding can postpone the compressor stall and the design point can be closer to the peak of the pressure rise, the compressor performance will be greatly boosted.

The process of stall inception is one of the hottest topics in the field of turbomachinery unsteady flow. Numerous studies have shown that the fluid dynamics mechanism of stall inception is identical regardless how the compressor stalls. It is closely related to the tip clearance flow. Hoying (10) examined the influence of three-dimensional flow structures within a compressor blade passage to determine the mechanism in rotating stall inception. They found that the stall inception depends on the stability of tip clearance leakage vortex. Vo (11) studied the impact of blade passage flow on the compressor

stability. He summarized two criteria for the subsonic compressor stall inception: tip clearance flow spillage below blade tip at the leading edge and backflow at the trailing edge blade tip. Hah (12) described the process of rotating stall inception in transonic rotor as follows: after the passage shock fully detached from the blade leading edges, the tip clearance vortex moves forward along the passage and the reversed tip clearance flow develops at the trailing edge, then the tip clearance flow spills below the leading edge. The research results indicated that tip clearance flow spillage and backflow at the trailing edge are flow behaviors directly related to stall inception. Analysis of their causes reveals that the mainstream axial momentum decreases together with the compressor flow coefficient. Meanwhile, the passage exit pressure increases as well as the blade load, forcing the tip leakage vortex turn to the adjacent blade pressure surface, thus traverses the blade passage. High adverse pressure gradient separates the flow and produces backflow region at the trailing edge. In this process, the potential affection of the increasing passage flow blockage further reduces the flow velocity of the mainstream, increases the incidence angle and intensifies the adverse pressure gradient acting on the leakage vortex. As a result, the interface of the tip clearance and oncoming flows keep moving forward until its leading edge coincided with the rotor's. This is when the compressor begins to stall. Therefore, the blockage of tip passage caused by the leakage vortex movement and the backflow at the trailing edge are the principle causes of stall inception (13, 14).

Air bleeding can remove low-energy fluid from critical regions of end-wall and ease the flow blockage. The flow mechanism has been widely used in external and internal flow control since Prandtl's boundary suction experiment in 1904. Now the air can be extracted from the rotor casing according to the location of blockage caused by leakage vortex movement and the trailing backflow. Could this bleeding plan give the compressor a larger stall margin by reducing the blockage of tip passage and inhibiting tip clearance flow spillage and the trailing backflow? This paper tries to explore an effective air bleeding method that can ensure a good compressor performance while providing air system with enough air to use.

NUMERICAL ANALYSIS PLAN

LOW SPEED SINGLE STAGE COMPRESSOR

The research object of this paper is the low-speed single stage compressor of Beijing University of Aeronautics and Astronautics (BUAA), as shown in Fig.1a). It consists of 19 rotors and 13 stators. The design mass flow rate is 2.40m^3/s at a rotational speed of 3000 rpm, providing a total pressure rise of 1500 Pa. The rotor tip radius is 225mm and the hub/casing ratio is 0.75, with a rotor tip clearance of 0.25mm. The Reynolds number is about 2×10^5 based on rotor tip chord. Details of the compressor geometry, operating conditions, and experimental data can be found in (15). Some information concerning the compressor stage is given in Table 1.

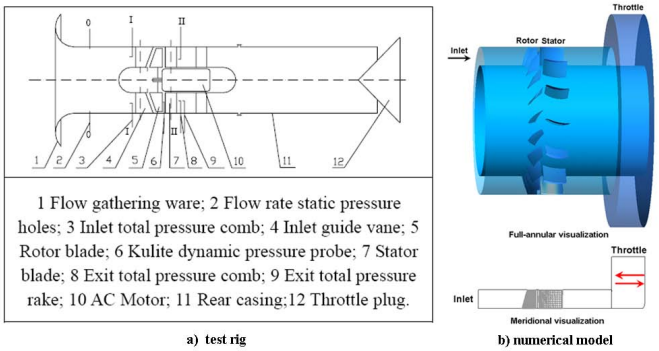

a) test rig b) numerical model

Fig.1 Schematic layout of the test rig & numerical model

Table 1 Design parameters of low speed axial compressor

Rotor RPM at 100% Speed	3000
Tip Speed (m/s)	70.7
Hub-Tip Radius Ratio	0.75
Number of Rotor Blades	19
Number of Stator Blades	13

NUMERICAL MODEL

In this simulation, the experimental measurements section at the inlet of compressor is selected for the calculation field boundary. Throttle device is set at the downstream of the compressor outlet about two times chord of the Stator. The entire design speedline between choke to stall can be simulated through the throttle movement. The numerical model is shown as Fig.1b). The space discretization of the compressor mesh is generated by the pre-processing module AutoGrid5. A butterfly grid topology is used on both rotor and stator, which consists of an inner H-type core portion encapsulated by an O-type grid domain. Local mesh is refined near the wall so as to ensure that the first layer from the solid wall grid to meet the $y^+<5$. In order to save a part of the computational effort required, the grid is optimized and total mesh points number is about 600,000. Full annular of three-dimensional computational mesh is shown in Fig.2. Simulations of the unsteady, three-dimensional viscous flow field are carried out on the compressor, using the three-dimensional Navier-Stokes (3DNS) code which solves the Reynolds-averaged Navier-Stokes (RANS) equations based on finite volume method. High-resolution scheme is used to solve the continuity equation, momentum equation and energy equation. Upwind scheme is used to solving turbulent kinetic energy and turbulent kinetic energy dissipation equation. The turbulence model of two-equation k-Epsilon is used for the present study. The rotor position changes with the physical time step in the unsteady numerical simulations. Ten physical time steps are set in one pitch, corresponding to 10 different relative angular

positions of the rotor to the stator. It takes about 1.0526×10^{-4} second for the rotor to complete a physical time step. The whole simulation lasts about 1 second, during which the rotor turns 50 rounds. The Transient Rotor-Stator is applied to the rotor/stator interface.

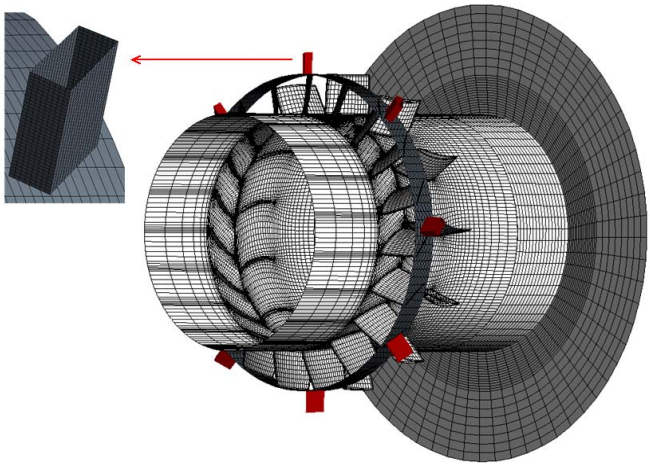

Fig.2 Structure of 3D computational mesh & bleeding slots

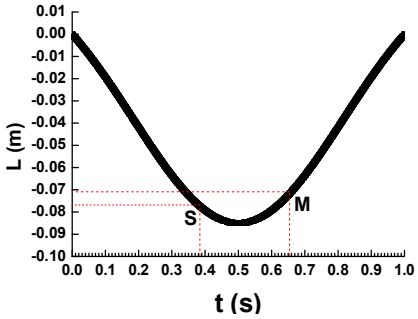

Fig.3 Control pattern of throttle in unsteady calculation

In the simulation, the atmospheric pressure and temperature of experimental environment are held as inlet boundary condition, respectively 102,510 Pa and 285.15 K. The atmospheric pressure is also held as outlet boundary condition. Similar to the throttling in experiment, the axial position of the throttle plug is changed using the moving mesh technology to obtain the characteristic line of compressor in the simulation. How throttle plug changes with the simulation time is shown in Fig.3. In this figure, t is the simulation time, and L is the axial displacement of the throttle. Negative L means the throttle is moving against the compressor axial direction. The result is similar to the throttling in experiment. The throttle closes slowly from 0 to 0.5 second. When the throttle moves to the S-point (t=0.3878 s) in the graph, the throttle position corresponds to the compressor stall inception. The throttle is opening slowly between 0.5 ~ 1.0 second. When the throttle moves next to the M point (t=0.6562s), the compressor recovers from stall. As the throttle opens wider, the compressor finishes the throttling state and returns to the simulated initial state. Between the S point and the M point, the throttle first closes until the compressor falls into the deep stall. Then the throttle slowly opens and the compressor enters the hysteresis loop. During this process, the throttle movement always keeps a rather low velocity.

BLEEDING PLAN

The location of the bleeding slot is designed near the blade trailing edge on the rotor casing, for the blockage of tip passage is caused by the leakage vortex movement and the backflow at the trailing edge is located downstream of the passage near the trailing edge. Eight bleeding slots are evenly distributed along the circumferential direction. The length and the width are about 50% and 25% respectively of the rotor tip chord. The structure of bleeding slots is shown in Fig.2. According to the analysis above, the plan is designed to remove the blockage of tip passage generated by the leakage vortex movement and the backflow at the trailing edge, increase the mass flow at the inlet, reduce the incidence angle, and delay the interface between the tip clearance and oncoming flows from moving forward.

The bleeding slots are modeled using standard H-grid. Taking into account the convergence of simulation, the mesh number in the slots is smaller than the number of the main flow passages. The bleeding slots are located in the stationary coordinate system. The boundary which connects the bleeding slots with the rotor casing is treated as transient Rotor-Stator. In the simulation, mass flow rate is held as the outlet boundary condition of the bleeding slots. The bleeding rate is 1% of the compressor main flow at design point.

ANALYSIS ON THE RELIABILITY OF UNSTEADY NUMERICAL SIMULATION

COMPARATIVE ANALYSIS ON THE OVERALL PERFORMANCE BETWEEN THE UNSTEADY SIMULATION AND EXPERIMENT WITHOUT BLEEDING

A comparison of the compressor characteristic over the 100% speedline without bleeding between unsteady numerical simulation and experimentally measured value is shown in Fig.4. In this paper, compressor characteristics of numerical calculations and experiment have been conducted non-dimensionalized by reference values: the abscissa Φ is the inlet flow coefficient V_x/U_m, and the ordinate Ψ is the total pressure rise coefficient $\Delta P^*/\rho U_m^2$. In order to describe more clearly, the compressor characteristics corresponding to the closing and opening throttle are drawn individually. The solid line with arrows is used to show the average trends of the total pressure rise in the stall region where the total pressure rise fluctuates very much. It is clear that on the design point (Ψ=0.325), the total pressure rise coefficient curve of unsteady calculation passes through the experimental data points. At the near-stall point (Φ=0.464), the total pressure rise of unsteady

calculations and experiments reach the maximum at the same time. Compressor characteristics of total pressure rise of unsteady calculations and experiments agree well with each other from choke to stall conditions. The hysteresis loop obtained through the throttle movement after the stall inception in unsteady numerical simulation is in accordance with the experimental results. The slight difference between the shapes of the two hysteresis loops is mainly due to the different shapes and moving speeds of the throttle in the calculation and experiments.

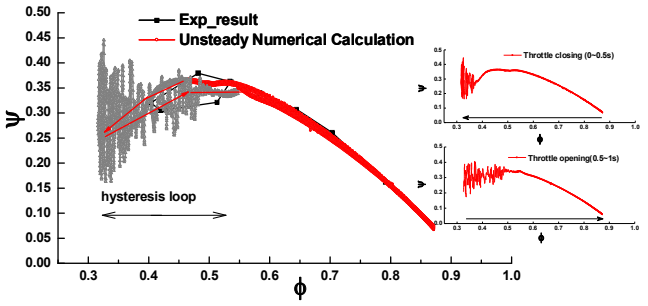

Fig.4 Comparison between the unsteady calculation and experimental results of the total pressure rise without bleeding

The above analysis shows that unsteady simulation calculation results are very close to the experiment measured results. In other words, the unsteady numerical calculation can reproduce the experimental results very approximatively, and the discrepancy is small enough to be ignored. Therefore, the compressor unsteady simulation without bleeding can be used as the baseline to study the influence of bleeding on the compressor overall performance by the numerical simulation.

CRITERIA FOR COMPRESSOR SURGE MARGIN IN NUMERICAL SIMULATION

The definition of numerical stall point in this paper is almost the same as (11, 16). When the compressor reaches its maximum static pressure rise, the interface between the tip clearance leakage and oncoming flows reaches the leading edge plain. So the maximum static pressure rise point coincides with the near-stall point. The Surge Margin calculation formula is as follows:

$$SM = \left(\frac{\Delta P_s^* / M_s}{\Delta P_d^* / M_d} - 1 \right) \times 100\% \quad (1)$$

SM is short for Surge Margin. M_s and ΔP_s^* represent the flow rate and total pressure rise at the near-stall point. M_d and ΔP_d^* stand for the flow rate and total pressure rise at design point.

ANALYSIS ON THE NEAR-STALL FLOW FIELD OF BASELINE

Flow field analysis of a near-stall compressor without bleeding (baseline) can show the internal flow within a compressor approaching stall point, and reflect how the stall is induced. Figure 5 is the curve of total pressure rise variation with the throttle control pattern. In the Figure, 5 points are selected as A, B, C, D, and E. Point A (Φ=0.618, t=0.3s) is the operating point of large flow rate. Point B (Φ=0.542, t =0.34s) is the design point. Point C (Φ=0.464, t=0.3878s) is the near-stall point. Point D (Φ=0.388, t 0.4249s) is the state point after stall inception, and the point E (Φ=0.332, t=0.4666s) is picked from the deep stall state. Analysis of instantaneous flow field at these points can reflect the development of a compressor from the design condition to stall inception and finally into the deep stall.

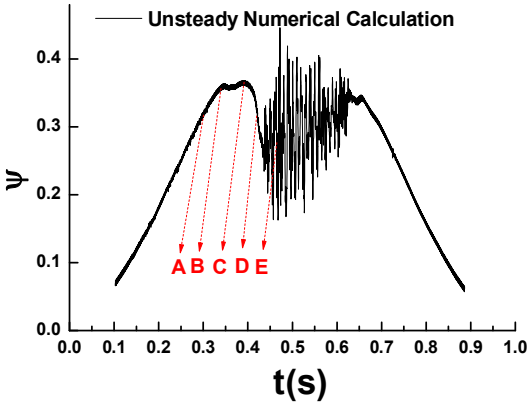

Fig.5 Curve of total pressure rise variation with the throttle control pattern

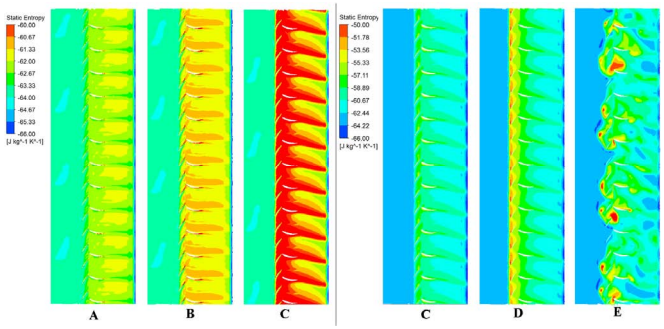

Fig.6 Entropy contours at 95% span at point A, B, C, D and E

Figure 6 is the entropy contours at 95% span of the point A, B, C, D and E. Instantaneous flow field of A, B and C can reflect the development of a compressor from the design condition to the stall inception. At point A, clearance leakage flow enters the passage at the 30% of chord and flows downstream as affected by the mainstream, and exits the passage near the adjacent blade trailing edge. In the tip flow field at this point, the axial momentum of the mainstream plays a dominant role in the confrontation with the clearance leakage flow. At point B, clearance leakage flow enters the passage at the 20% of chord. The blade load increases and pushes the tip leakage vortex to the pressure surface of the

adjacent blade, and traverses the downstream blade passage. In the tip flow field at this point, the axial momentum of the mainstream begins to decrease, and the location where clearance leakage flow enters the passage begins to move upstream. The blockage of tip passage generated by the leakage vortex movement starts to accumulate in the downstream passage. At point C, the interface between the tip clearance leakage and oncoming flows reaches the leading edge plain. Tip leakage flow traverses the blade passage at the rotor inlet and the blockage of tip passage increases sharply. At this point, influenced by the potential affection of the tip passage, the axial momentum of the mainstream continues to decrease and the tip leakage flow takes over the dominant place in tip passage. The incidence angle of rotor increases and the compressor starts to stall.

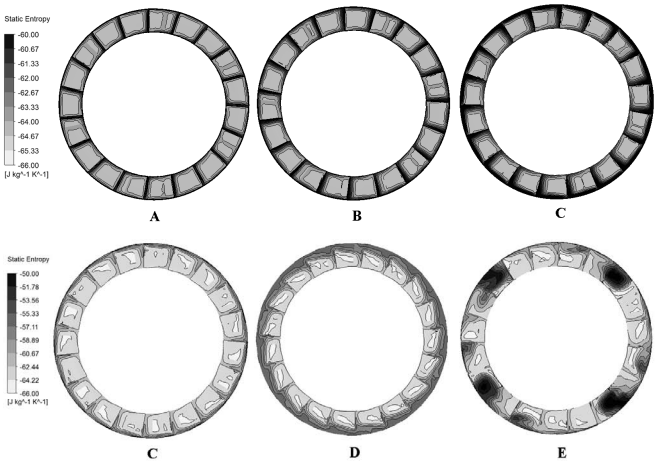

Fig.7 Rotor exit entropy contours at point A, B, C, D and E

Instantaneous flow field of C, D and E reflect how the compressor develops from the stall inception to the deep stall. Figure 7 is the entropy contours at rotor exit at point A, B, C, D and E. It is clear that at point C, a great range of high-entropy area forms at the trailing edge of rotor. Just as the analysis above concluded, the flow begins to separate and a recirculation area appears at the trailing edge due to the high adverse pressure gradient in the passage. Losses and blockage of tip passage further increases. At this point, the compressor stalls. Blockage and losses of passage concentrate in the casing corner near the trailing edge of the rotor suction surface, and flow field above 80% of the rotor span is affected. As the flow coefficient decreases, the effect of backflow at the trailing edge and blockage is passed on to the upstream. The tip leakage flow grows stronger and the flow field of tip passage aggravates. At point D, the loss regions of the rotor tip expand fast and occupy the entire rotor pitch range, thus leave no room for the mainstream to enter. Meanwhile, the scope of the flow blockage and loss caused by stall rapidly expands. It covers the area above 60% of the rotor span at the exit, and runs through the entire circumferential range. With the flow coefficient decreasing, 4 large stall cells have formed along the circumferential at point E. Each span 4 pitches in circumferential. The cells completely block the whole passage in the radial, and rotate at a rate of 50% of rotor speed in the same direction with the rotor. The compressor now is in the deep stall.

The unsteady simulation result of the compressor without bleeding shows that, the blockage of tip passage caused by the leakage vortex movement and the backflow at the trailing edge are major causes for stall inception at low flow rate. Blockage and losses of tip passage concentrate in the casing corner near the downstream passage. This blockage spreads downstream, disturbing the flow of downstream stators, and results in a deterioration of compressor performance. Next part of this paper will explore how bleeding influences the tip flow field, and how the stall occurs and develops using the unsteady simulation of the compressor with bleeding.

ANALYSIS OF THE IMPACT OF THE BLEEDING ON THE COMPRESSOR PERFORMANCE

INFLUENCE ON TOTAL PRESSURE RISE AND SURGE MARGIN

Total pressure rise and surge margin are two major performance parameters for low speed axial compressor. However, the compressor stability can hardly be maintained without compromising the total pressure rise. The comparison below is between the overall characteristics of the bleeding plan and the baseline. It tries to explore a way to improve both the total pressure rise and SM at the same time.

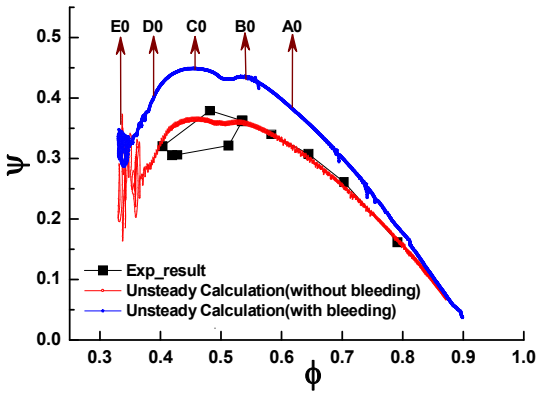

Fig.8 Overall characteristics of the non-dimensionalized flow coefficient and the total pressure rise in bleeding plan

Figure 8 shows the overall characteristics of the non-dimensionalized flow coefficient and the total pressure rise in bleeding plan. To compare with the experimental results and unsteady simulation results without bleeding, the inlet flow coefficient and the total pressure rise coefficient between compressor inlet and outlet are selected to analyze the bleeding impact on the compressor performance, excluding the internal

flow of the bleeding slot. Table 2 lists out the relative increment of stability margin in bleeding plan. The surge margin in the baseline calculation is 19.42%. According to Fig. 8 and Table 2, the total pressure rise and surge margin in this bleeding plan both see great enhancement. Within the range between the choke and the stall, the smaller the inlet flow rate, the greater the total pressure rise. The total pressure rise on the design point (Φ=0.542) grows by 22.1% than the baseline. The flow rate on the stall point (Φ=0.454, t=0.3976s) reduces slightly after bleeding, and the mass flow range expands by only 1.87%. Influenced by the total pressure rise significantly enhanced after bleeding, the surge margin reaches 23.38%, which is a 20.4% increase on the baseline. Figure 9 shows how the total pressure rise changes with the throttle control after bleeding. It can be seen that stall onset here occurs 0.0106s later than in the baseline, during which the rotor makes half a round. Although bleeding does not delay the stall inception much, but the oscillation amplitude of the total pressure rise after stall significantly declines, which accounts for less than 16% of local average total pressure rise compared with 45% in the baseline.

Table 2 Relative increment of stability margin in bleeding plan

Plan	Bleeding Rate	SM	ΔSM %
Experimental	—	20.38%	—
Without Bleeding	—	19.42%	—
Bleeding	1%	23.38%	20.4%

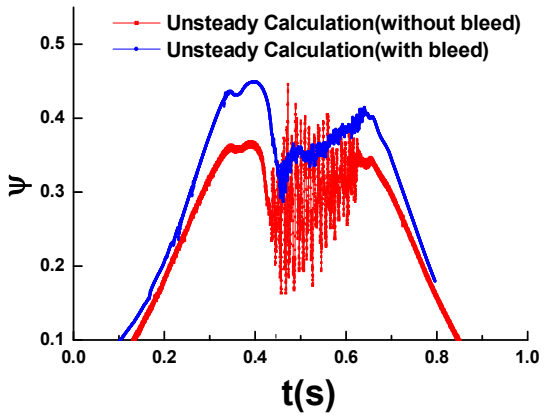

Fig.9 Curve of total pressure rise variation with the throttle control pattern after bleeding

The analysis of the impact of bleeding on the total pressure rise indicates that, when the compressor operates at constant rotation speed, appropriate bleeding design can stabilize the flow, improve the performance and expand surge margin from choke to stall onset. Therefore, reasonable air bleed can enhance compressor surge margin while ensuring a continuous air supply. It also proves that it's totally feasible to combine air system bleeding with compressor flow control to get a better compressor performance.

INFLUENCE ON ROTOR TIP FLOW FIELD AND STALL PROCESS

Analysis on rotor flow field with bleeding can show how bleeding affects the internal flow within a rotor. In the Figure 8, 5 points are selected as A0 (Φ=0.618), B0 (Φ=0.542), C0 (Φ=0.464), D0 (Φ=0.388) and E0 (Φ=0.332), correspond to the five points A, B, C, D and E in Figure 5. Analysis of instantaneous flow field at these points can reflect the impact of bleeding on the rotor tip flow field and the outgrowth of stall.

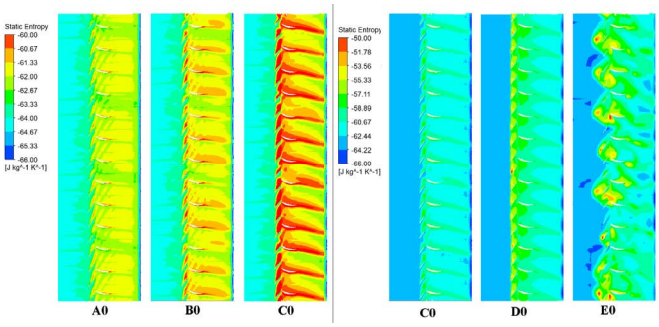

Fig.10 Entropy contours at 95% span at point A0, B0, C0, D0 and E0

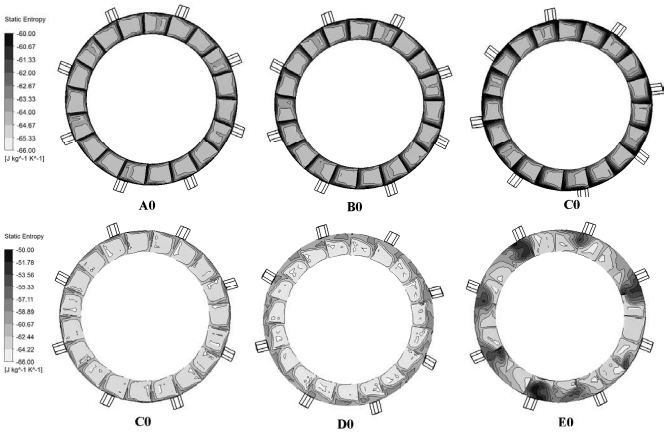

Fig.11 Rotor exit entropy contours at point A0, B0, C0, D0 and E0

Figure 10 is the entropy contours at 95% span at point A0, B0, C0, D0 and E0. Figure 11 is the entropy contours at rotor exit at point A0, B0, C0, D0 and E0. Instantaneous flow field at A0, B0 and C0 can reflect that bleeding can effectively ease the blockage of tip passage near the bleeding slot, inhibiting tip clearance flow spillage and the trailing backflow. Particularly at point C0, the blockage of the blade passage near the bleeding slot significantly diminishes. The radial range and the flow loss of the annular boundary layer also decline near the rotor trailing edge. Figure 12 shows the radial distribution of the circumferentially-averaged relative total pressure loss

and outlet flow angle of the near-stall rotor. Figure 13 shows the radial distribution of the circumferentially-averaged entropy production of the near-stall rotor. Entropy production of numerical calculations has been conducted non-dimensionalized by reference values: the abscissa S is the entropy production coefficient 100×ΔE/Cp, and the ordinate is the radial location. As shown in these figures, the relative total pressure loss and outlet deviation angle is significantly improved in the area above 80% of the blade span after bleeding. There is a great reduction in the flow loss, in the region above 90% of the blade span the reduction can be as much as 50%. Now there is a larger main flow in the tip region as the blockage has eased and loss has declined. Meanwhile, the interface of the tip clearance and oncoming flow moves slower toward the leading edge of rotors.

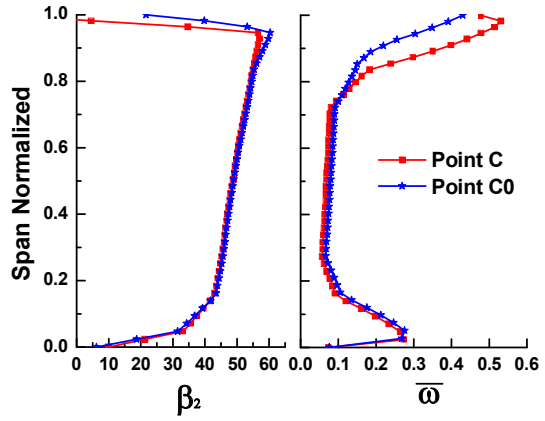

Fig.12 Radial distribution of the circumferentially-averaged relative total pressure loss and outlet flow angle of the near-stall rotor

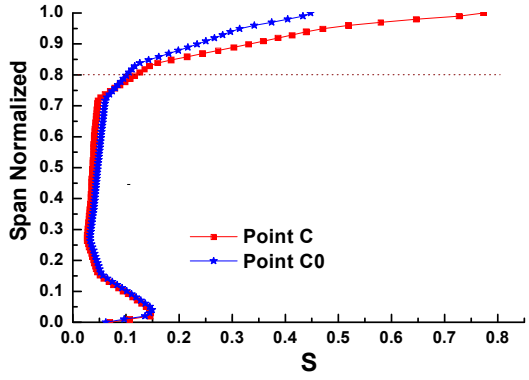

Fig.13 Radial distribution of the circumferentially-averaged entropy production of the near-stall rotor

Instantaneous flow fields at C0, D0 and E0 reflect the impact of bleeding on the compressor after the stall inception. At point D0, bleeding has effectively inhibited the expansion of the loss region at the rotor tip, and the tip passage begins to see more air flow. At point E0, 4 original stall cells along the circumferential become less intensified and influential under the effects of bleeding. According to Figure 6, 7, 10, and 11, the number of stall cells grows to 6 from 4. Each spans across 2 pitches in circumferential, and the radial range under their influence shrank. The flow loss caused by stall cells also declines.

It can be concluded that the blockage and flow loss caused by the leakage vortex movement and the backflow at the trailing edge can be reduced effectively by bleeding. Although the smaller blockage and loss manage to improve the tip flow and postpone the stall onset, the stall still cannot be prevented. However, bleeding contributes to the rotor flow field in reducing the flow loss and improving the inlet flow environment of the downstream stator. The total pressure rise thus obtains a great increase. The primary reason of substantial enhancement of the compressor total pressure rise is the improvement of the tip flow field of the rotor.

influence on the downstream stator

From Figure 10 and 11, it is clear that bleeding has significantly improved the downstream stator tip field. As the bleeding slot is located near the blade trailing edge on the rotor casing, the local backflow and blockage are reduced, the rotor exit trail is weakened, and the movement of separation and the leakage vortex to downstream stators is slowed down. As a result, the stator passage loss is reduced. Particularly at point B0, C0 and D0, the flow loss in the stator passage substantially decreases, leading to an increase in the mainstream flow rate of the stator tip region. Figure 14 compares the circumferential distribution of the time-averaged stator inlet flow angle at 95% span in one rotor rotational period near the stall point between the bleeding plan and the baseline. The abscissa is the circumferential location of the stator, and the ordinate is the inlet flow angle. It can be seen that the inlet flow angle of the stator in the tip region is significantly reduced by bleeding, and the average inlet flow angle reduces from the 69 degrees in the baseline to the 61.5 degrees in the bleeding plan. It means that the incidence angle of the stator in the tip region decreases by 7.5 degrees. The stator flow field is therefore greatly improved.

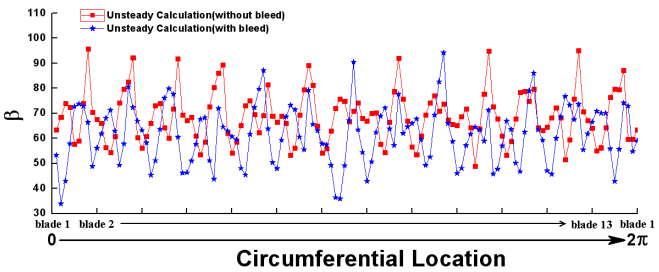

Fig.14 Circumferential distribution of the time-averaged inlet flow angle at 95% of span of the near-stall stators

In the stator flow field, the mainstream flow rate increases because the blockage and loss at rotor tip area is reduced by bleeding on the rotor casing. As this effect is passed downstream, the incidence angle of the stator in the tip region decreases, the flow loss of the stator passage is significantly reduced. Consequently, the total pressure rise of the compressor is substantially boosted.

CONCLUSIONS

This paper takes the single stage and low speed axial compressor as the research object, develops a time-accurate numerical method on the compressor overall performance by using the moving mesh to simulate the function of compressor throttle plug. Combined with experimental results, compressor flow field with and without air bleeding are compared and analyzed to study the impact of bleeding on compressor performance. The conclusions are as follows:

1) Air bleeding can effectively reduce the blockage and flow loss in the tip passage caused by the leakage vortex movement and the backflow at the trailing edge, and slows down the movement of the interface of the tip clearance and oncoming flows to the rotor leading edge. As a result, the incidence angle of stator in tip region decreases significantly. The total pressure rise in turn grows sharply.

2) The plan in which 1% of the air is extracted from rotor casing near trailing edge succeeds in raising both the total pressure rise and surge margin of compressor at the same time. Compared with the baseline condition, the total pressure rise increases by 22.1%, flow range expands by 1.87% and the overall surge margin rises by 20.4%.

ACKNOWLEDGMENTS

This work was supported by a grant from the National Natural Science Foundation of China (No. 60934001).

REFERENCES

[1] Andrew, J. Y. and Ronald, J. R.,1992, “Effects of Bleed Air Extraction on Thrust Level of the F404-GE-400 Turbofan Engine,” NASA TM-104247.

[2] Alison, B. E., 1991, “The Effects of Compressor Seventh-stage Bleed Air Extraction on Performance of the F100-PW-220 Afterburning Turbofan Engine,” NASA CR-179447.

[3] Zhao, B., Li, S.B., Hou, A.P., and Zhou, S., 2009, “The Research on Air Bleed of Air System in Aero-engine,” Academic Exchanging Meeting of 15th Turbomachinery Committee of Aviation Institute, pp. 190-198.

[4] Wellborn, S. R., and Michael, L. K., 2002, “Bleed Flow Interactions with an Axial-Flow Compressor Powerstream,” AIAA Paper 2002-4057.

[5] Leishman, B. A., Cumpsty, N. A., and Denton, J. D., 2007, “Effects of Bleed Rate and Endwall Location on the Aerodynamic Behavior of a Circular Hole Bleed Off-Take,” ASME Journal of Turbomachinery, 129, pp. 645–658.

[6] Leishman, B. A., Cumpsty, N. A., and Denton, J. D., 2007, “Effects of Inlet Ramp Surfaces on the Aerodynamic Behavior of Bleed Hole and Bleed slot Off-Take Configurations,” ASME Journal of Turbomachinery, 129, pp. 659–668.

[7] Leishman, B. A., and Cumpsty, N. A., 2007, “Mechanism of the Interaction of a Ramped Bleed Slot with the Primary Flow,”ASME Journal of Turbomachinery, 129, pp. 669–678.

[8] Gummer, V., Goller, M., and Swoboda, M., 2008, “Numerical Investigation of End Wall Boundary Layer Removal on Highly Loaded Axial Compressor Blade Rows,” Journal of Turbomachinery, 130(011015), pp. 1~9.

[9] Dobrzynski, B., Saathoff, H., Kosyna, G., Clemen，C., and Gummer, V., 2008, “Active Flow Control in a Single-Stage Axial Compressor Using Tip Injection and Endwall Boundary Layer Removal,” ASME Paper, GT 2008-50214.

[10] Hoying, D. A., Tan, C. S., Vo, H. D. et al., 1999, “Role of blade passage flow structures in axial compressor rotating stall inception,” ASME Journal of Turbomachinery, 121, pp. 735-742.

[11] Vo, H. D., Tan, C. S., and Greitzer, E. M., 2005, “Criteria for Spike Initiated Rotating Stall,” ASME Paper, GT 2005-68374.

[12] Hah, C. Bergner, J., and Schiffer, H., 2006, “Short length-scale rotating stall inception in a transonic axial compressor-criteria and mechanism,” ASME Paper, GT2006-90045.

[13] Adamczyk, J. J., Celestina, M. L., and Greitzer, E. M., 1993, “The Role of Tip Clearance in High-Speed Fan Stall,” ASME Journal of Turbomachinery, 115, pp. 28-38.

[14] Wu, Y. H., Chu, W. L., and Lu, X. G., 2006, “The Effect of Tip Leakage Flow Structure on Compressor Aerodynamics,” Chinese Journal of Engineering Thermophysics, 27(6), pp. 950-952.

[15] Li, Z. P., Li, Q. S., Yuan, W., Lu, Y. J., Jiang, H.B., 2006, “The Experimental Research on a New Method for Extending the Axial-Compressor s Stall Margin,” Chinese Journal of Aerospace Power, 21 (3), pp. 485-491.

[16] Camp, T. R., and Day, I. J., 1998, “A Study of Spike and Modal Stall Phenomena in a Low-Speed Axial Compressor,” ASME Journal of Turbomachinery, 120, pp. 393-401.